

Decadal-resolution record of winter monsoon intensity over the last two millennia from planktic foraminiferal assemblages in the northeastern Arabian Sea

The Holocene
1–16
© The Author(s) 2015
Reprints and permissions:
sagepub.co.uk/journalsPermissions.nav
DOI: [10.1177/0959683615591357](https://doi.org/10.1177/0959683615591357)
hol.sagepub.com


Philipp M Munz,¹ Michael Siccha,² Andreas Lückge,³
Anna Böll,⁴ Michal Kucera² and Hartmut Schulz¹

Abstract

The Indian monsoon system is an important climate feature of the northern Indian Ocean. Small variations of the wind and precipitation patterns have fundamental influence on the societal, agricultural, and economic development of India and its neighboring countries. To understand current trends, sensitivity to forcing, or natural variation, records beyond the instrumental period are needed. However, high-resolution archives of past winter monsoon variability are scarce. One potential archive of such records are marine sediments deposited on the continental slope in the NE Arabian Sea, an area where present-day conditions are dominated by the winter monsoon. In this region, winter monsoon conditions lead to distinctive changes in surface water properties, affecting marine plankton communities that are deposited in the sediment. Using planktic foraminifera as a sensitive and well-preserved plankton group, we first characterize the response of their species distribution on environmental gradients from a dataset of surface sediment samples in the tropical and sub-tropical Indian Ocean. Transfer functions for quantitative paleoenvironmental reconstructions were applied to a decadal-scale record of assemblage counts from the Pakistan Margin spanning the last 2000 years. The reconstructed temperature record reveals an intensification of winter monsoon intensity near the year 100 CE. Prior to this transition, winter temperatures were $>1.5^{\circ}\text{C}$ warmer than today. Conditions similar to the present seem to have established after 450 CE, interrupted by a singular event near 950 CE with warmer temperatures and accordingly weak winter monsoon. Frequency analysis revealed significant 75-, 40-, and 37-year cycles, which are known from decadal- to centennial-scale resolution records of Indian summer monsoon variability and interpreted as solar irradiance forcing. Our first independent record of Indian winter monsoon activity confirms that winter and summer monsoons were modulated on the same frequency bands and thus indicates that both monsoon systems are likely controlled by the same driving force.

Keywords

Indian paleomonsoon, late Holocene, planktic foraminifera, sea surface temperature, transfer functions, winter monsoon intensity

Received 29 November 2014; revised manuscript accepted 24 April 2015

Introduction

The monsoon climate is generally defined as the seasonal reversal of the prevailing surface winds and accompanied precipitation, driven by the migrating low surface pressure belt of the Intertropical Convergence Zone (ITCZ) and atmospheric pressure over Central Asia (Wyrki, 1971). In the Arabian Sea region, strong and moisture-laden southwesterly winds prevail during summer, when the low-pressure zone of the Hadley circulation is on the northward position over continental Asia and northern Arabia (Shetye et al., 1994). The reversed mode during winter drives dry northeasterly winds of lower velocity toward the low-pressure zone above the open ocean. Both seasonal modes of the monsoon lead to distinct hydrographic changes in the water column of the Arabian Sea, affecting the production and distribution of marine plankton, including planktic foraminifera (Curry et al., 1992; Schiebel et al., 2004; Schulz et al., 2002). Southwesterly winds during summer induce upwelling by Ekman transport along the coast of Somalia, Oman, and southwestern India, resulting in enhanced primary production and surface water cooling from

June to September (Colborn, 1975; Currie et al., 1973). North-easterly winter winds cause cooling of surface waters in the northeastern Arabian Sea, and the resulting deepening of the thermocline and weakening of the thermal stratification enable convective mixing and injection of nutrients into the photic zone (Banse and McClain, 1986; Ittekkot et al., 1992; Madhupratap et al., 1996). In the northeastern Arabian Sea, these processes lead to maximum primary productivity during winter (Lückge et al.,

¹Department of Geosciences, University of Tübingen, Germany

²MARUM – Center for Marine Environmental Sciences, Germany

³Bundesanstalt für Geowissenschaften und Rohstoffe (BGR), Germany

⁴Institute of Geology, University of Hamburg, Germany

Corresponding author:

Philipp M Munz, Department of Geosciences, University of Tübingen, Hölderlinstr. 12, 72074 Tübingen, Germany.
Email: philipp.munz@uni-tuebingen.de

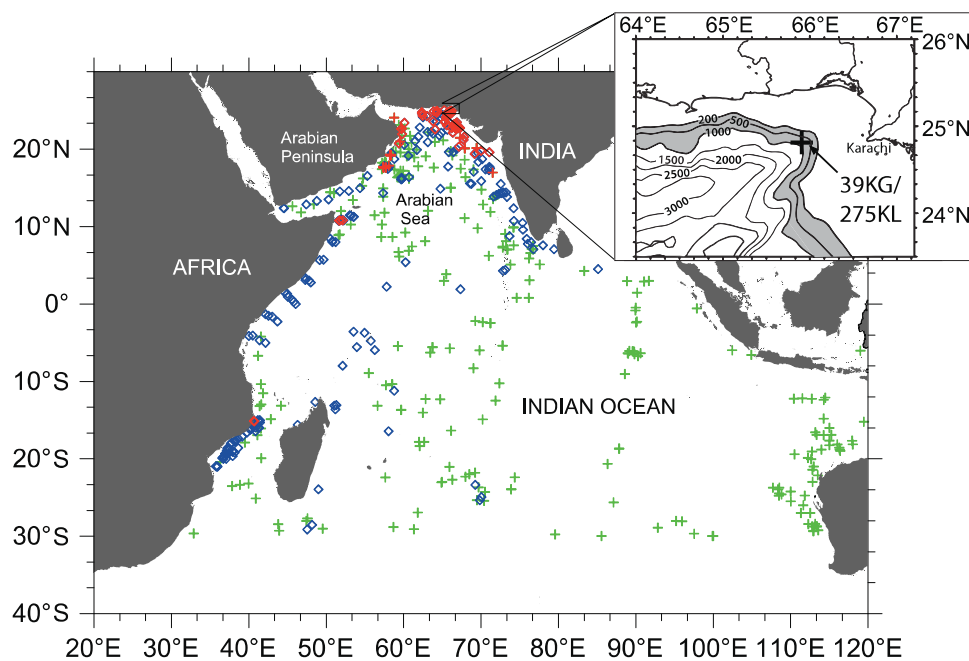


Figure 1. Map of the Indian Ocean showing locations of core top samples of the initial calibration dataset. Cross symbols are samples from the AUSMAT-F4 dataset compiled by the MARGO group ($n=329$; Barrows and Juggins, 2005). Open diamond symbols are the additional $n=274$ from this study. Red colored symbols were used for the reconstruction in the adjusted calibration dataset. Inset map shows the location of cores 39KG/275KL on the upper continental margin off Pakistan, within the permanent oxygen minimum zone (gray shading) on the Makran accretionary wedge.

2002; Schulz et al., 2002). Sediment trap studies revealed a conspicuous shift of the planktic foraminiferal (PF) assemblage induced by these two particular oceanic seasons (Curry et al., 1992; Schulz et al., 2002), indicating that PF may be a powerful recording system for past dynamics of the Indian monsoon.

Historical records of past Indian monsoon intensity are limited to the last ~140 years (Sontakke et al., 1993), therefore limiting the accurate determination of low-frequency multi-decadal- to centennial-scale variability of the monsoon system. The time frame over the last two millennia (the Common Era, CE) provides the opportunity to disentangle natural climate variability from anthropogenic forcing (e.g. Jones and Mann, 2004) and has recently attracted broad attention of the scientific community (PAGES 2k Consortium, 2013). The dynamics of the summer monsoon over the last two millennia have been intensively studied from speleothem records on the Arabian Peninsula, Socotra, and Andaman Islands (Burns et al., 2002; Fleitmann et al., 2003, 2007; Laskar et al., 2013; Neff et al., 2001); marine sediments recording upwelling intensity off Oman (Anderson et al., 2002; Gupta et al., 2003); and tree rings from localities in Central Asia and on the Indian subcontinent (Bräuning and Mantwill, 2004; Cook et al., 2013; Xu et al., 2012).

But the dynamics of the winter monsoon are virtually unknown. In theory, an anti-phase behavior to the summer monsoon intensity can be derived from the lateral migration of the annual mean position of the ITCZ. On millennial and longer timescales, a more northward position of the ITCZ induces strengthening of the summer monsoon and weakening of the winter monsoon during interstadials, whereas the situation during stadials is reversed (Wang et al., 2005a; Yancheva et al., 2007). On decadal to centennial timescales, however, both systems are probably controlled by the dynamics of the El Niño/Southern Oscillation (ENSO; Kumar et al., 2006; Zhou et al., 2007). To better predict how the summer and winter monsoon interact and whether they respond in-phase and coherently to external forcing, long records of the winter monsoon are needed.

The upper continental slope off Pakistan (Figure 1) is characterized by a strong and permanent oxygen minimum zone (OMZ)

between a water depth of 200 and 1200 m (Schulz et al., 1996; von Rad et al., 1995), resulting from mid-water oxygen consumption by high degradation rates of organic matter. Oxygen deficiency prevents post-depositional mixing of the sediment by burrowing organisms, which enables the formation and preservation of annually resolving varve-like laminated sediments (Lückge et al., 2001; Schulz and von Rad, 2014; Schulz et al., 1996, 2002). High sedimentation rates caused by high biological productivity as well as the lateral advection and resuspension of fine-grained terrigenous matter (Schulz and von Rad, 2014), combined with the lack of bioturbation, enables the identification of interannual and even seasonal signals (Kemp, 1996). This makes marine sediments from the OMZ on the Makran accretionary wedge off Pakistan an archive of an exceptionally high-resolution chronology, providing the potential to unravel short-term climate oscillations. Compared to the northwestern Arabian Sea, where sea surface temperatures (SST) are coldest during summer upwelling, minimum SST along the coast off Pakistan occurs during the winter season (Figure 2). This suggests, verified by satellite-derived concentrations of monthly chlorophyll *a* in the surface waters (Feldman and McClain, 2013), that the annual cycle of sea surface properties in this area is dominated by winter conditions.

In a previous paper (Böll et al., 2014), we attempted to reconstruct winter monsoon intensity from regionally calibrated alkenone temperatures and stable nitrogen isotopes in laminated sediment cores (39KG/275KL) from the Pakistan margin (Figure 1). There, we identified a general cooling trend of reconstructed annual mean temperatures (AM-SST) over the last 2400 years together with several periods of century-scale temperature changes that occurred largely in phase with geochemical productivity estimates. However, open questions about the response of surface water properties to winter monsoon activity remained when the general trend of decreasing temperatures and increasing productivity was reversed, for example, during the ‘Medieval Warm Period’ (‘MWP’) (950–1250 CE; CE/BCE was used numerically equivalent to AD/BC). Furthermore, we observed a heterogeneous pattern of coccolith and alkenone fluxes from a

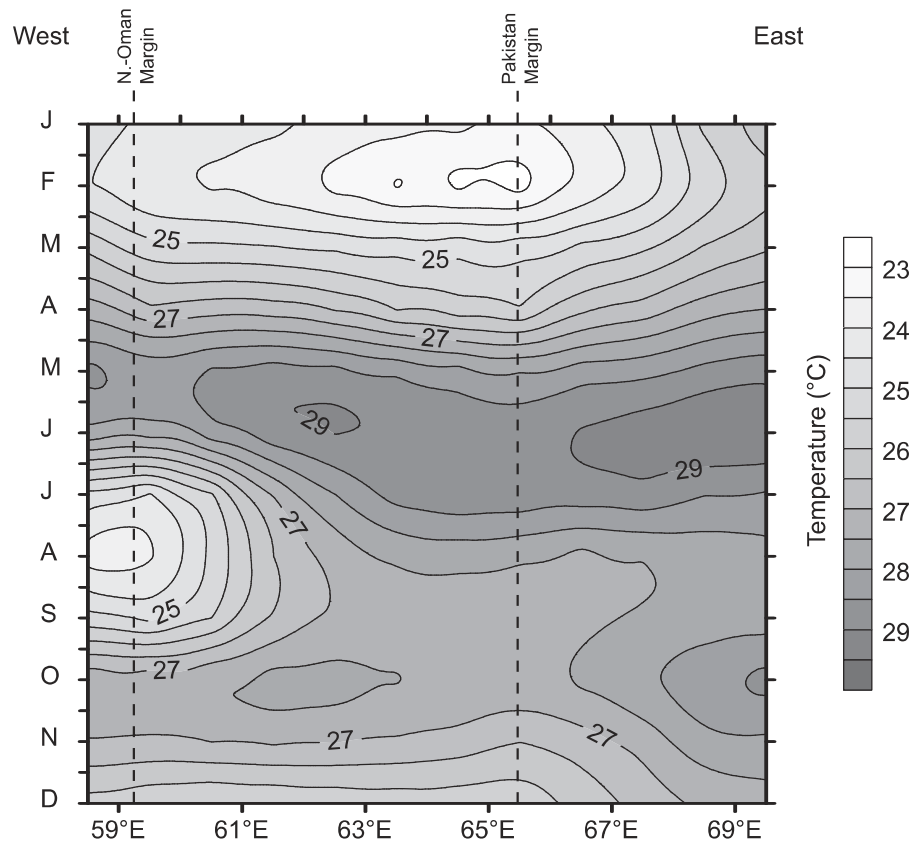


Figure 2. Contour plot of annual (January–December) temperature evolution along an arch-shaped section in the northern Arabian Sea in the approximate depth of cores 39KG/275KL, showing lowest temperatures off Pakistan during winter and off Oman during summer.

sediment trap study over the course of 1 year. Because the observed seasonality greatly contributes to the general difficulty in attributing alkenone-derived AM-SST to the seasonal winter component, we have used the same sediment cores in this study (39KG/275KL) and generated a high-resolution record of PF assemblages spanning the last 2000 years. Using a new, regionally valid transfer function constrained by rigorous evaluation of potential driving forces, we convert the assemblage counts into a record of winter sea surface temperatures (wSST). This record is then used to assess the seasonal evolution of winter monsoon variability in the northeastern Arabian Sea and to allow comparison with other proxy records of winter and summer monsoon intensity. This allows a rigorous investigation of a potential anti-phase relationship to the summer monsoon during the late Holocene.

Material and methods

Late Holocene sediment record from the Pakistan margin

In order to calculate SST variations over the last 2000 years from foraminiferal transfer functions, we studied samples from the uppermost 15 cm of Sonne 90 box-core 39KG (von Rad et al., 1995, 1999) and the uppermost 167 cm of Sonne 130 piston-core 275KL (Böll et al., 2014; von Rad et al., 1998). Both cores were taken at the same station from the continental margin off Pakistan (Figure 1; 24°50'N, 65°55'E, 695 m water depth), allowing us to achieve a continuous record over the last 2000 years. Correlation of both cores was enabled by a 10 cm-thick reddish-brown event layer ('F1-layer'), present in both records (Schulz and von Rad, 2014). Coarse fraction samples of box-core 39KG above F1 were available in continuous 3-mm intervals ($n=50$ samples) from a previous study (Doose-Rolinski et al., 2001). 275KL was sampled from a U-Channel below F1 in continuous 5 mm intervals

($n=332$ samples) to achieve a suitable number of PF individuals from the narrower sample size.

Chronostratigraphy of both cores has been presented by von Rad et al. (1999), who established age models of Sonne 90 cores 39KG and 56KA by varve counts and conventional and AMS radiocarbon dating. Correlation between 56KA and 275KL, recovered at the same location, is based on a layer-by-layer tracking of prominent 1- to 30-mm-thick light colored event deposits ('C-Layers'). 39KG covers the record from retrieval in the year 1993 CE to the deposition of F1 in 1888 CE, providing an average sample resolution of 2 years for the last ~100 years. 275KL is linked to the record of 39KG below F1 and was analyzed from 1888 CE until 118 BCE with an average resolution of 9 years for the last ~2000 years.

Samples for PF analyses were freeze-dried, wet-sieved over a 63-μm screen, and oven-dried at 40°C. Counts were conducted on a split fraction (39KG) or the whole residue (275KL) of the size fraction >150 μm, examined under a stereo-dissecting microscope. Planktic foraminifera were identified to species level, based on the taxonomic framework given by Bé (1967, 1977) and Hemleben et al. (1989). For the calculation of relative assemblage compositions of 275KL, samples yielding less than 300 counted individual PF were combined with adjacent samples to achieve a minimum of 300 individuals. A total of 89 samples were merged, representing 27% of the dataset. Merging was done when the coarse fraction of a sample was diluted by fine-grained terrigenous matter of an event deposit ('C- or F-Layers'), thus not decreasing the actual resolution of the marine deposition.

Surface sample calibration dataset

To investigate factors affecting assemblage composition of planktic foraminifera in surface sediments in the Arabian Sea, we compiled modern core top data consisting of a subset of the

AUSMAT-F4 dataset compiled by the MARGO group ($n=329$ samples; Barrows and Juggins, 2005), extended by $n=274$ new samples by this study. The subset was defined to cover the tropical and sub-tropical Indian Ocean from 30°N to 30°S and from 30° to 120°E , to reduce the risk of including endemic species and cryptic morphotypes from divergent oceanic environments. According to Kucera et al. (2005b), noise in the data could be introduced by a broader geographical coverage, when the genetic and ecological variation not captured by the taxonomic input variables increases, and with the increasing influence of secondary environmental gradients. Because of the unique environmental forcing in the Bay of Bengal (Murty et al., 1992; Wyrtki, 1973) and the Red Sea (Auras-Schudnagies et al., 1989; Siccha et al., 2009), samples from these basins were omitted. The $n=274$ additional samples substantially increased the regional coverage of the eastern and northeastern Arabian Sea and along the western margins of the Indian Ocean (Figure 1).

Both datasets were thoroughly checked for taxonomic inconsistencies and for an adequate minimum number of identified PF individuals. Assemblage alteration by carbonate dissolution was identified by unusually high numbers (>3%) of the dissolution-resistant species *Sphaeroidinella dehiscens*. To minimize a potential bias introduced by different contributors to the dataset, taxonomic units showing a close morphological similarity, namely, *Globigerinella siphonifera* and *Globigerinella calida* (Weiner et al., 2015), as well as *Globorotalia menardii* and *Globorotalia tumida*, were merged, respectively. All morphotypes of *Globigerinoides sacculifer*, with and without a sacc-form ultimate chamber, were treated as one taxonomic unit (André et al., 2013). Because of the low signal-to-noise ratio of rare species for quantitative paleoenvironmental reconstructions (Kucera et al., 2005b), the dataset was filtered to a minimum average occurrence of 0.5%. This resulted in the exclusion of 14 out of 29 species.

For the construction of an adjusted calibration dataset, a joined R-mode principal component analysis (PCA) was conducted. Since measurements of the input variables are based on the same units (relative species abundances), a covariance matrix was used to preserve the magnitude of variation between the variables (e.g. Ramette, 2007). A log-ratio transformation was used to compensate for the mutual dependency of the compositional dataset (Aitchinson, 1999; Aitchinson et al., 2000). PCA was conducted on log-transformed relative abundances of the 15 species in the initial pool of tropical and sub-tropical Indian Ocean surface samples ($n=603$) and the downcore faunal dataset (Figure 3). The first two principal component (PC) axes explained 61% of the variance of both datasets. $N=103$ samples in the calibration dataset had the same range of PCA scores along the first two PC axes as the downcore samples, thus being most similar in the direction of the first two components. The remaining $n=500$ calibration samples described assemblages not represented in the downcore dataset, most likely recording conditions outside of the range of variation of the winter monsoon region.

To investigate the species response to potential controlling environmental gradients, a redundancy analysis (RDA) was carried out using the VEGAN package (Dixon, 2003) of the R statistical program (R Core Team, 2014). Since the annual cycle of plankton productivity in the investigated area of the eastern Makran is dominated by winter conditions (Madhupratap et al., 1996), and specimens of PF deposited during winter therefore dominate the sedimentary assemblages, we calibrated the modern core top database to variables representing the boreal winter season (J-F-M and D-J-F).

Since the Arabian Sea experiences extreme intraannual variations of biological productivity (Banse, 1987; Lal, 1994; Prasanna Kumar et al., 2001; Smith et al., 1998; Zeitschel and Gerlach, 1973), three different approaches were made to characterize the primary production. As a proxy for the surface standing stock of

phytoplankton, chlorophyll *a* measurements from NASA's SeaWiFS and MODIS sensors were used (Feldman and McClain, 2013). The December to February averages were binned over a timespan from 1998 to 2010. In comparison, Vertical Generalized Production Models (VGPM) calculate net primary production rates in the euphotic zone (Behrenfeld and Falkowski, 1997), taking into account the physiological variability through the water column. We employed the Eppley-version VGPM as a temperature-dependent model of photosynthetic efficiency extracted from the Ocean Productivity Site (2014) to generate an estimate of winter productivity. As an additional approach of quantifying phytoplankton productivity, we applied the updated Carbon-based Production Model (uCbPM; Ocean Productivity Site, 2014), which, compared with VGPM, calculates phytoplankton carbon biomass from particulate backscatter coefficients and is independent of standard chlorophyll measurements. Both net primary productivity estimates were calculated as January–March averages from 1998 to 2010. As a measure of water column stratification, the maximum Brunt–Väisälä frequency (BVF) of the top 250 m of the water column was used. The calculations were performed on the data of the World Ocean Atlas 2001 (Conkright et al., 2002) using the implemented algorithm in *OceanDataView* 4.5.7 (Schlitzer, 2014). SST is apparently the strongest determinant controlling PF species distributions in large parts of the world's oceans (Morey et al., 2005). Following the MARGO recommendations (Kucera et al., 2005a), SST values were interpolated via kriging to the core top samples from the 10 m depth level of the World Ocean Atlas 2001 (Conkright et al., 2002). We are aware of a potential bias introduced by PF assemblages that are more sensitive to subsurface than to surface temperatures, as discussed by Telford et al. (2013). However, we do not expect large changes in the ocean thermal structure over the last 2000 years and consider this issue to be of less importance here. In total, the PF assemblage data in the adjusted surface dataset are then analyzed together with five environmental parameters, reflecting winter productivity (chlorophyll *a*, Eppley-VGPM, uCbPM), temperature (SST), and stratification (BVF).

Design of the transfer function models

We used a suite of different transfer functions for the quantitative reconstructions of environmental variables controlling the distribution of planktic foraminifera. There is no single 'best method' to be recommended (Juggins and Birks, 2012), and using different statistical techniques that model species response to environmental gradients in different ways allows the assessment of signals that are robust to method-specific bias (Kucera et al., 2005b), which is particularly significant in our case where we expect a relatively low signal-to-noise ratio. We employed the Imbrie and Kipp factor analysis – IKFA (Imbrie and Kipp, 1971), weighted averaging partial least square regression – WA-PLS (ter Braak and Juggins, 1993), the maximum likelihood response curves method – MLRC (Birks et al., 1990), and artificial neural networks – ANN (Malmgren and Nordlund, 1997). Except for ANN, we used the R package *rioja* ver. 0.8-7 (Juggins, 2013) to calculate the transfer functions. All methods used the relative species abundances of the adjusted calibration dataset ($n=103$ samples). As a measure of distance to modern analogs, the Bray–Curtis dissimilarity to the samples of the adjusted calibration dataset was calculated for each fossil sample. For IKFA, the number of factors to extract was determined by the Kaiser–Guttman criterion and Parallel Analysis after Horn (1965), both limiting the number of factors to five. For WA-PLS, two components performed with the lowest error during cross-validation and were thus used for the reconstruction. ANN were computed as back propagation networks using the *BioComp* software *NeuroGenetic Optimizer*® ver. 2.6.142. The system was configured to limit the number

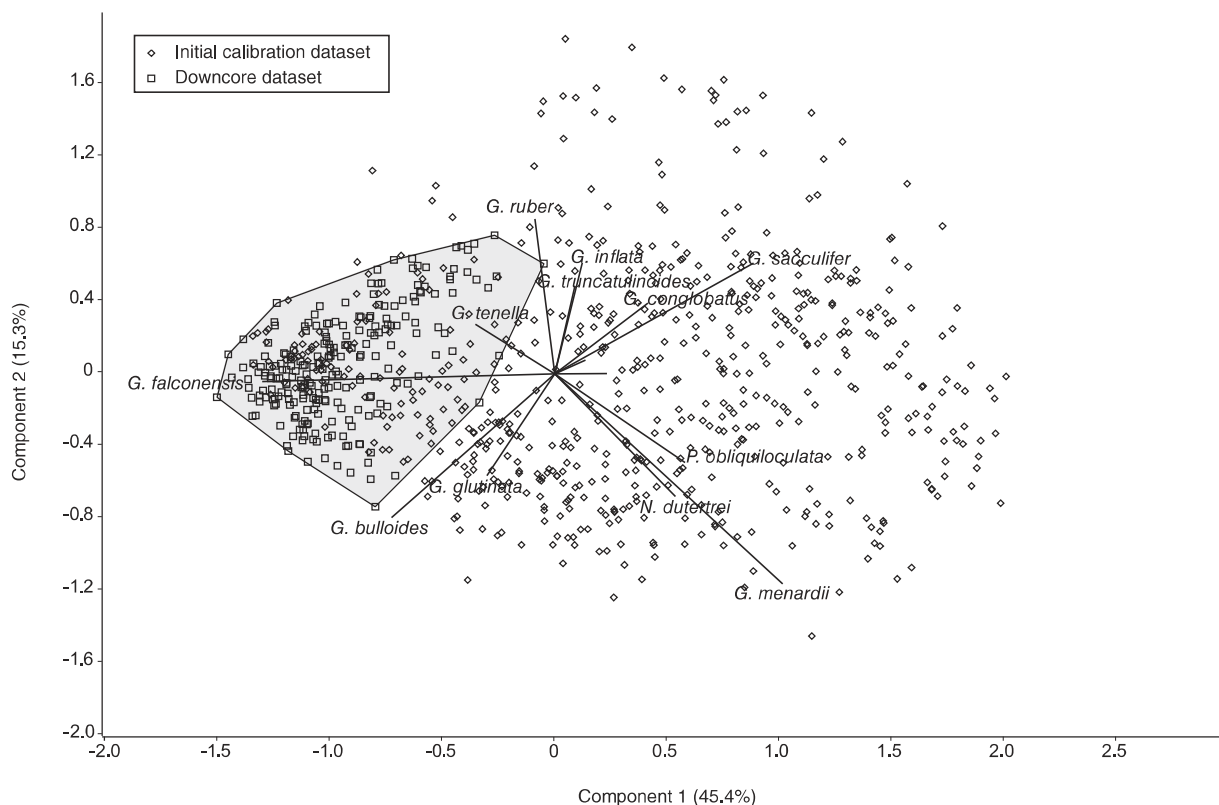


Figure 3. Joint PCA scatter plot and species scores of the log-transformed calibration (diamond) and downcore (square) datasets. The gray shaded area marks the variability captured by the late Holocene record of cores 39KG/275KL, defining the final input for calibrating the transfer functions.

of neurons in multiple hidden layers to four and to optimize the network structure with 100 network populations over 30 generations, with a minimum of 100 and a maximum of 2500 passes, and a stop criterion if no improvement occurred over the last 40 passes.

Performance fitness was based on improvement of the root mean square error (RMSE) of a test set, consisting of 50% of the surface sample dataset. Ten different pairs of training and test sets were used, and the average of the best of the 10 resulting networks was calculated as the final output. Except for ANN, model validation and error estimates were based on bootstrapping (1000 cycles). Root mean square error of prediction (RMSEP) was estimated from the cross-validated average RMSE across the bootstrap cycles. The sample-specific standard error of prediction was calculated as the square root of the sum of the samples' squared standard error and the mean squared error across the bootstrap cycles. ANN RMSEP was calculated from the average RMSE across the 10 best networks.

Results

Modern faunal distribution and multivariate analysis of the surface sample dataset

The distribution of PF species in the surface sample dataset (Figure 4) replicates the patterns observed by Bé and Hutson (1977) and Hutson and Prell (1980). The increased spatial coverage in the northern Arabian Sea, along the margin off Oman and western India, as well as off Somalia and Mozambique, allows for a more detailed analysis. *Globigerinoides ruber* (white), the most abundant species in the entire calibration dataset, is most frequent below the sub-tropical gyre of the southern Indian Ocean and south of the central Arabian Sea. Furthermore, *G. ruber* is abundant along the western coast of India outside the Gulf of Khambat. *Globigerina bulloides* shows highest abundances close to the

coast of high summer upwelling areas off northern Somalia and Oman, as well as off the southwestern tip of India. Medium abundances are apparent along the entire coast off Somalia, in the Gulf of Aden, as well as in the northern and eastern Arabian Sea. *Globigerinoides glutinata*, on the other hand, seems to be more abundant outside the coastal upwelling areas in the open-ocean upwelling of the northern Arabian Sea. *Neogloboquadrina dutertrei*, *G. sacculifer*, and *G. menardii* are typical for the central Arabian Sea and for open-ocean sites along the South Equatorial Current. *N. dutertrei* occurs in low numbers along the coast of Somalia, Oman, and southwest India, but is not found in the northeastern Arabian Sea. *G. sacculifer* is also absent in surface samples from the western and northeastern Arabian Sea (see also Schulz et al., 2002). *G. siphonifera/G. calida* is, like *G. sacculifer*, mostly absent from regions of intense upwelling and occurs in moderate numbers in the open equatorial and southern Indian Ocean. Very high numbers of *G. menardii/G. tumida* observed in a few open-ocean sites might be an indication for calcite dissolution. *Globigerina falconensis* seems to be characteristic of the eastern and northeastern Arabian Sea.

Results of the RDA conducted on the adjusted calibration dataset with the winter constraints are illustrated as a triplot in Figure 5. The first axis explains 38.9% of the variation in the species data and is highly correlated with temperature, stratification, chlorophyll *a* concentration, as well as the Eppley-VGPM productivity (Table 1). The second axis, explaining 16.3% of the species variation, is correlated strongest with the uCbPM.

Among the environmental variables investigated by RDA, winter temperature (wSST) has the highest correlation with the first axis and thus appears to be the most important variable for the explanation of the species variation. Temperature and stratification are positively correlated with each other, and the pair is negatively correlated to chlorophyll *a* and Eppley-VGPM. Relative abundances of *G. siphonifera*, *Globotruncana rubescens*, and *G. sacculifer* show a positive correlation with increasing

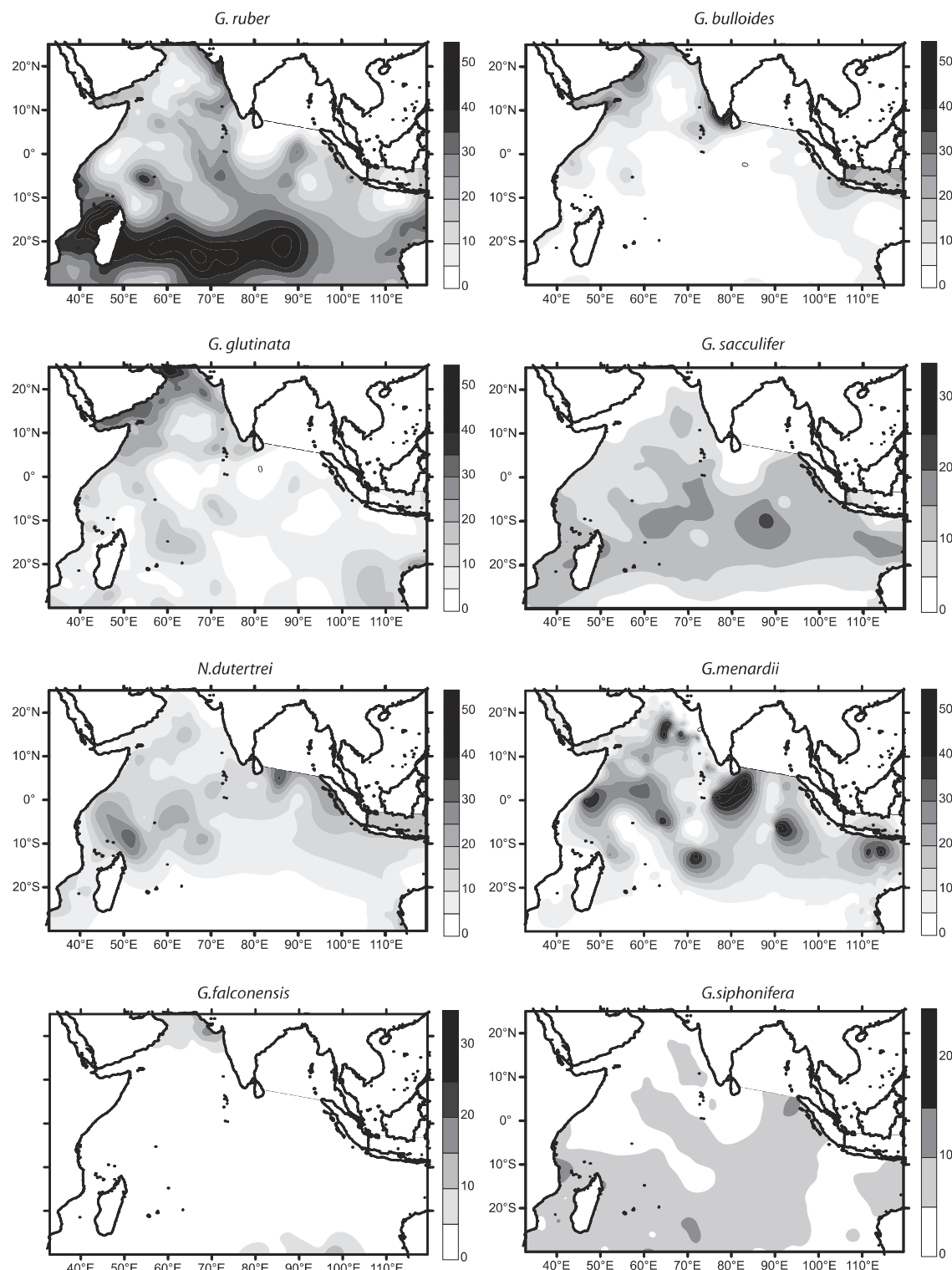


Figure 4. Contour plot of relative frequencies of species >3% average abundance in initial core top database spanning the Arabian Sea and Indian Ocean from 30°N–30°S and 30°E–120°E, by omitting the Bay of Bengal and the Red Sea.

temperatures and stratification and a negative correlation with chlorophyll *a* and Eppley-VGPM. Stratification is correlated with the relative abundances of *G. menardii* and *N. dutertrei* and has a negative correlation with *Globoturborotalita tenella*. Interestingly, uCpPM best explains the abundance of *G. falconensis*, *Turborotalita quinqueloba*, and *G. ruber* and to a minor extent also of *G. glutinata*. *G. bulloides* plots on the positive end of the second RDA axis and implies a negative correlation with the winter productivity of the uCpPM model. Stronger winter winds cause intensified cooling, winter deep mixing, and enhanced primary productivity (Banse and McClain, 1986; Madhupratap et al.,

1996). Accordingly, stronger winter conditions shift the faunal assemblage from *G. bulloides* to higher abundances of *G. falconensis* and *G. glutinata*.

Transfer function performance

One of the key assumptions of paleoecological transfer functions states that the environmental variable to be reconstructed is the dominant factor for the ecological changes in the fossil assemblage records (e.g. Juggins and Birks, 2012). Thus, we reconstructed the gradient that performed best in explaining the species variation by

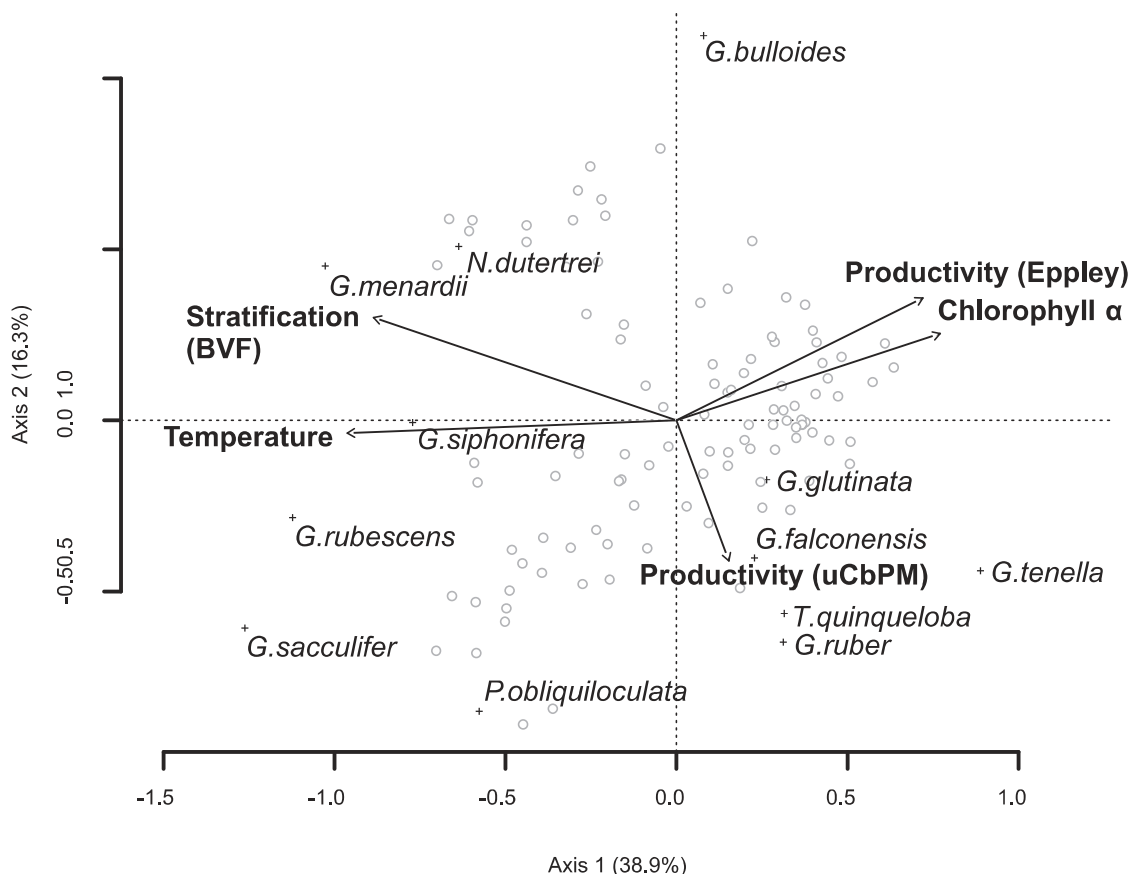


Figure 5. Scatter triplot of redundancy analysis results computed with the species (cross symbols) and environmental data (arrows) of the winter season. Open circles indicate surface samples.

Table I. Results of the redundancy analysis of the adjusted calibration dataset.

	RDA1	RDA2	RDA3	RDA4	RDA5	Permutation test statistics (p)
Eigenvalue	0.389	0.163	0.100	0.050	0.010	
Cumulative proportion explained	0.115	0.163	0.192	0.207	0.210	
Correlation						
Temperature	-0.982	-0.038	-0.005	0.081	0.169	<0.001
Stratification	-0.903	0.307	-0.293	-0.005	0.071	<0.001
Chlorophyll a	0.786	0.259	0.437	-0.193	0.294	<0.01
Eppley-VGPM	0.735	0.365	0.555	-0.085	0.107	<0.01
uCbPM	0.156	-0.419	-0.113	0.776	0.431	<0.01

VGPM: Vertical Generalized Production Models; uCbPM: updated Carbon-based Production Model.

RDA, which is wSST. In terms of reconstruction uncertainties, WA-PLS and IKFA showed similar error rates and outperformed MLRC (Table 2). The error estimation of ANN is not based on bootstrapping and is therefore not fully comparable with the other techniques. In general, all prediction error estimates are considerably lower than the uncertainty for basin-wide foraminiferal transfer functions of 1–2°C (e.g. Kucera et al., 2005b). Error estimates represent a minimum uncertainty because the training and test sets are not fully independent and contain a certain degree of spatial autocorrelation (Telford and Birks, 2005; Telford et al., 2004). However, since the selection criterion for the final calibration dataset is based on taxonomic similarity rather than geographically or environmentally close sites, samples are distributed among different margins of the Arabian Sea (Figure 1). To compare the absolute values of the error rate with basin-wide reconstructions, these are expressed as the percentage of the range of the target variable (Table 2). Values range from 15.4%, 17.6%, and 18.6% for ANN,

WA-PLS, and IKFM, respectively, to 24.9% for MLRC. This is about three to four times higher compared with basin-wide reconstructions with a target variable range of ~30°C (e.g. Kucera et al., 2005b). This reflects the fact that basin-wide datasets have a very strong temperature dependency in the middle part of the SST gradient, whereas our adjusted calibration dataset is at the edge of the SST gradient. The initial subset of the calibration dataset covering the tropical and sub-tropical Indian Ocean exhibits a range of the wSST gradient of 18–29°C, whereas the adjusted dataset exhibits a range of 23–27°C.

Downcore development of PF assemblages

It turned out that high species variability of the biennial resolution record of core 39KG is not comparable with the decadal-scale resolution of the longer core 275KL (Supplementary Figure S1, available online). As a consequence, we would expect this to

Table 2. (a) Error estimates for the individual transfer functions reconstructing wSST and (b) correlation table among the individual reconstructions and with PC1 scores (lower left corner shows in bold numbers the linear correlation value r , upper right corner represents the respective p value).

	(a) Error estimates for transfer functions				(b) Correlation among reconstructions				
	RMSE	RMSEP (bootstrap)	R^2	Range fraction of the target variable (%)	WA-PLS	IKFM	MLRC	ANN	PC1 scores
WA-PLS	0.545	0.632	0.505	17.55		2.04E-53	1.84E-67	4.50E-77	9.91E-16
IKFM	0.597	0.671	0.360	18.63	0.39		4.68E-47	1.57E-29	3.87E-65
MLRC	0.786	0.896	0.326	24.87	0.62	0.77		1.16E-45	8.45E-51
ANN	0.556		0.606	15.44	0.92	0.65	0.77		4.34E-37
PC1 scores	—	—	—	—	-0.50	-0.85	-0.79	-0.71	

RMSE: root mean square error; RMSEP: root mean square error of prediction; WA-PLS: weighted averaging partial least square regression; MLRC: maximum likelihood response curves method; ANN: artificial neural networks.

result in poor analogy to a calibration dataset of the same decadal-to centennial-scale resolution. For the purpose of this study, we therefore achieved a spliced record of comparable temporal resolution while retaining a continuous sampling scheme by binning the PF counts from 39KG to the average resolution of the longer core 275KL.

Eight PF species occurred with average abundances of >2%, that together sum up to 96% of the total faunal composition. These are in descending order: *G. falconensis*, *G. bulloides*, *G. ruber*, *G. glutinata*, *G. siphonifera*, *N. dutertrei*, *G. sacculifer*, and *G. tenella* (Table 3). A PCA conducted solely on the downcore dataset was used to investigate the major trends in the fossil fauna (Figure 6). The first component explains 40.6% of the total variance, and the second component explains 13.7%. The variance explained by the second component is lower than the variance generated by a broken-stick model and can therefore probably be neglected (e.g. Joliffe, 2002). The first axis mainly separates *G. sacculifer* and *G. siphonifera* from *G. tenella* and *G. glutinata*. PCA time series reveals that samples that are most associated with the former species occurred largely prior to the year 450 CE (Figure 7), consistent with higher abundances of *G. sacculifer* and *G. siphonifera*. Downcore development of PF species distribution is given in Figure 7. The most noticeable feature from the dataset is the occurrence of *G. sacculifer* between 250–450 CE and 100 BCE–100 CE, together with higher abundances of *G. siphonifera* and *Orbulina universa*. Whereas *G. sacculifer* is mostly absent after 450 CE, this species is reaching more than 25% prior to 450 CE. Simultaneously, *G. tenella* is rare or completely absent prior to 450 CE, and *G. falconensis* shows lower abundances during the interval 100 BCE to 100 CE.

A positive correlation among reconstructed wSST from all transfer function techniques and with the PC1 scores (Table 2) indicates that the ecological changes in the species assemblages are interpreted coherently by all methods and reflect the strongest gradient in the data. It is therefore very likely that the reconstruction is primarily driven by the changes of the reconstructed environmental variable (Juggins and Birks, 2012).

Discussion

Environmental control on species distribution

The results of RDA on the adjusted dataset of modern samples revealed a strong relationship along the first component between temperature and stratification on the one side and the chlorophyll-based productivity estimates on the other side (Figure 5). This might be explained by the mutual dependency of thermocline deepening and strength of surface cooling during the winter season. Stronger and colder surface winds lead to more severe cooling of surface waters and thus enhance convective winter deepening of the mixed layer. The less stratified water column enables nutrients from deeper waters to be mixed into the euphotic zone, nourishing

primary productivity. As a result, both effects cannot be fully disentangled. However, the positive correlation of *G. falconensis*, a species considered as typical for the deep thermocline mixing during winter monsoon conditions (Peeters and Brummer, 2002; Schulz et al., 2002), and other productivity-indicating species with increasing uCpPM productivity could indicate that these model data are a useful representation of nutrient conditions during winter monsoon. *G. bulloides* is considered as an indicator of summer upwelling conditions in the western Arabian Sea (Curry et al., 1992; Gupta et al., 2003; Naidu and Malmgren, 1996). The strong negative correlation of *G. bulloides* with winter productivity, especially uCpPM, reveals an anti-phase relationship of this species to winter conditions in this part of the basin. Possible lateral advection of nutrient-rich surface waters originating in the upwelling areas of the northwestern Arabian Sea (Schulz et al., 1996) could lead to higher accumulation rates of *G. bulloides* during summer. If *G. bulloides* is related to summer conditions, the response of this species could not be explained by the winter constraints of the analysis. The constrained variation explained by the second RDA component is, however, small compared with the total unconstrained variance, which makes to refrain from an attempt to construct a transfer function for winter productivity. *G. siphonifera* and *G. sacculifer* are associated with warmer temperatures and accordingly weaker winter conditions. Both species are spinose macroperforate, symbiont-bearing, and mainly occur in warm tropical and sub-tropical waters with low seasonality (Fraile et al., 2008; Hemleben et al., 1989). In the Arabian Sea, *G. sacculifer* and *G. siphonifera* are typical for non-upwelling areas of low nutrient concentrations (Cayre et al., 1999; Peeters and Brummer, 2002; Schiebel et al., 2004).

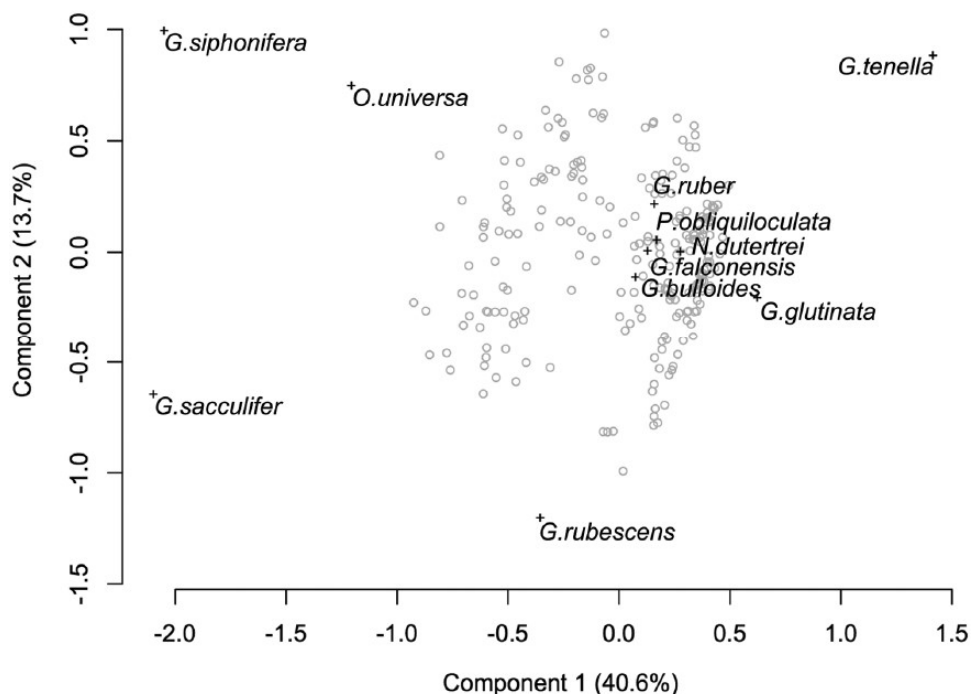
G. glutinata is common in coastal and open-ocean upwelling areas (Naidu and Malmgren, 1996) and known to feed mainly on diatom prey (Hemleben et al., 1989). In sediment trap studies of the northeastern Arabian Sea, *G. tenella* occurs together with *G. rubescens* during late winter and spring (Schulz et al., 2002). The negative association of the samples of this interval in the PCA of the downcore dataset with productivity-related species (*G. falconensis*, *G. bulloides*, *G. glutinata*) and the positive association with temperature-related *G. sacculifer* and *G. siphonifera* suggest diminished influence of winter monsoon conditions. After 450 CE, *G. sacculifer* occurs only sporadically in very small numbers, indicating a sudden faunal shift in the PF assemblage.

Decadal-scale variability of foraminiferal assemblages and winter monsoon intensity over the last two millennia

Given the relatively short period covered by the two core profiles 39KG and 275KL, most species show a comparatively high variability in their abundances (Table 3). A sampling interval of 5 mm corresponds to an average sediment accumulation time of

Table 3. Summary statistics of planktic foraminiferal abundances in the fossil record of cores 39KG/275KL.

Species	Mean	Minimum	Maximum	Standard deviation	Occurrence (total n=382)
<i>Globigerina falconensis</i> (Blow, 1959)	26.65	11.24	49.33	7.73	362
<i>Globigerina bulloides</i> (d'Orbigny, 1829)	23.07	7.17	47.24	7.11	356
<i>Globigerinoides ruber</i> white (d'Orbigny, 1839)	22.86	4.36	48.20	7.92	345
<i>Globigerinita glutinata</i> (Egger, 1895)	12.13	2.16	30.83	4.96	358
<i>Globigerinella siphonifera</i> (d'Orbigny, 1839)	2.80	0	15.61	3.31	255
<i>Globigerinella calida</i> (Parker, 1962)	0.19	0	2.43	0.27	56
<i>Globoturborotalita tenella</i> (Parker, 1958)	2.50	0	12.11	2.69	233
<i>Neogloboquadrina dutertrei</i> (d'Orbigny, 1839)	2.45	0	7.50	1.35	344
<i>Globigerinoides sacculifer</i> (Brady, 1877)	2.22	0	27.58	4.12	179
<i>Globoturborotalita rubescens</i> (Hofker, 1956)	1.41	0	10.53	1.50	232
<i>Pulleniatina obliquiloculata</i> (Parker and Jones, 1865)	1.10	0	4.39	0.80	272
<i>Orbulina universa</i> (d'Orbigny, 1839)	1.07	0	18.50	2.09	107
<i>Globorotalia menardii</i> (Jones and Brady, 1865)	0.69	0	3.24	0.58	195
<i>Neogloboquadrina pachyderma</i> (Ehrenberg, 1861)	0.21	0	2.09	0.35	55
<i>Turborotalita quinqueloba</i> (Natland, 1938)	0.18	0	2.73	0.42	43
<i>Dentigloborotalia anfracta</i> (Parker, 1967)	0.13	0	1.88	0.28	41
<i>Beella digitata</i> (Brady, 1879)	0.10	0	2.10	0.29	25
<i>Globigerinoides conglobatus</i> (Brady, 1879)	0.05	0	1.16	0.14	17
<i>Tenuitella iota</i> (Parker, 1962)	0.07	0	1.08	0.16	15
<i>Globorotaloides hexagonus</i> (Natland, 1938)	0.03	0	1.21	0.10	2
<i>Globorotalia theyeri</i> (Fleisher, 1974)	0.02	0	0.60	0.07	2
<i>Hastigerina pelagica</i> (d'Orbigny, 1839)	0.01	0	1.28	0.09	1
<i>Globoquadrina conglomerata</i> (Schwager, 1866)	0	0	0.42	0.03	1

**Figure 6.** Scatter plot of the downcore principal component analysis and the variance explained by each axis. The first principal component (PCI) mainly separates *Globigerinella siphonifera* and *Globigerinoides sacculifer* from *Globoturborotalita tenella* and *Globigerinita glutinata*.

~10 years. Occasional sampling of an unequal number of summer and winter layers could potentially lead to an irregular distribution of each season, which might introduce a noisy sampling bias of up to 10% disparity compared with a signal of equal seasons. If this were the case for our dataset, the similarity of the adjacent samples would be lower than the similarity to samples of increasing distance. For 66% of the dataset, the Bray–Curtis similarity to the closest sample is, however, higher compared with the similarity of the next-but-one sample. We therefore conclude that the observed variability of species abundances is not affected by an unequal contribution of the seasonal signals, but rather attests to

the success of the sampling scheme, which yielded decadal-scale data not affected by bioturbation mixing in the laminated sediments.

The high variability within the species dataset is also obvious from the scatter plot of the joint PCA of the downcore and entire initial calibration dataset (Figure 3). The latter is spanning a wide ecological range of the tropical and sub-tropical Indian Ocean, and thus contains most of the species variance. The downcore dataset covers approximately one-fourth of the variance captured by the initial calibration dataset. This suggests that short-term interannual fluctuations in PF relative abundances and production

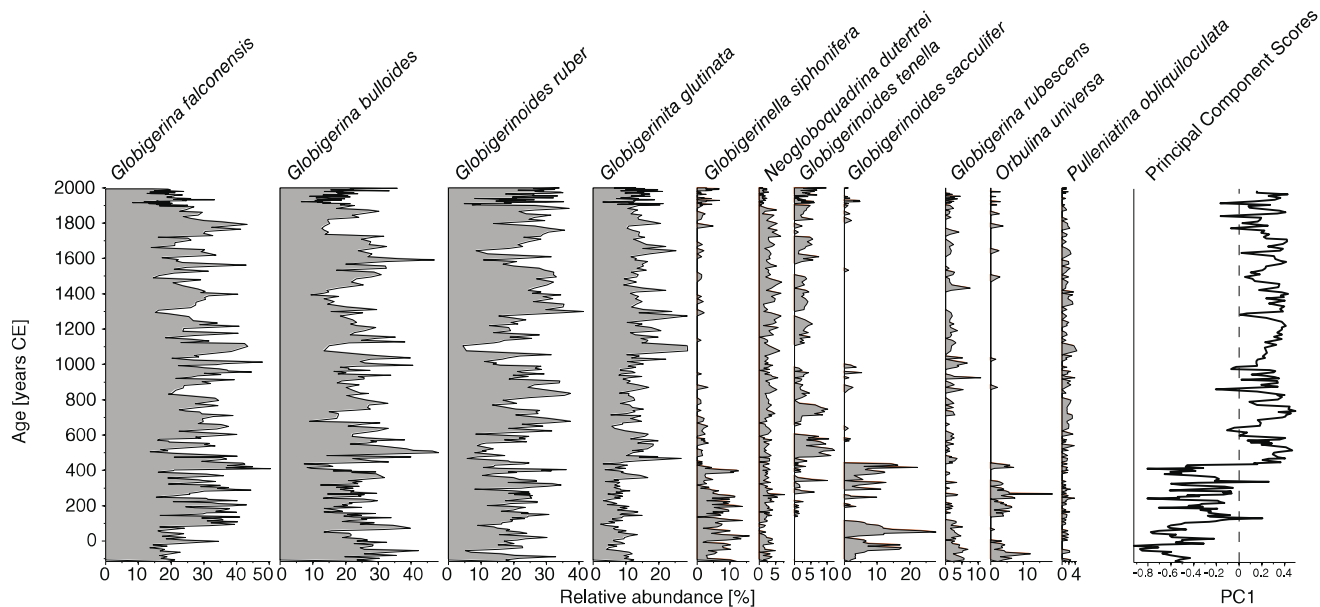


Figure 7. Changes in relative abundance of the planktic foraminiferal taxa and first principal component scores (from Figure 6) during the last ~2000 years in cores 39KG/275KL. The abrupt change at 450 CE is associated with the sudden occurrence of *Globigeroides sacculifer* and *Globigerinella siphonifera*, mainly on the expense of *Globoturborotalita tenella* and *Globigerinata glutinata*.

rates are underestimated by potentially bioturbated core top samples, often carrying an integrated signal over several decades to millennia (Kucera et al., 2005b).

The multi-decadal evolution of the wSST variance and detrended temperature anomaly (Figure 8) reveals that winter monsoon variability shows three stages of changing strength and frequency. Whereas during the periods prior to 250 CE and after 450 CE changes are relatively small, wSST variance during the period 250–450 CE was considerably higher. To further explore the decadal- to centennial-scale variability of the wSST record, we computed the spectral peaks with the multitaper method (MTM) implemented in the *SpectraWorks* software *kSpectra®* ver. 3.4.2 (Ghil et al., 2002) with the default settings ($p=2$, $K=3$ tapers). Figure 9 shows the MTM frequency spectrum of the detrended wSST time series, smoothed with a low-pass Butterworth filter with a 30-year cutoff frequency. Multi-decadal variability of winter monsoon intensity was found on 75-, 40- to 37-, and 31-year cycles. Several recent studies based on observational data (e.g. Kim et al., 2014; Krishnamurthy and Krishnamurthy, 2014; Webster et al., 1998; Zhou et al., 2007) indicated that the monsoon–ENSO relationship is modulated on low-frequency inter-decadal timescales according to regime shifts of the Pacific Decadal Oscillation (PDO). The PDO, defined as the leading mode of monthly SST anomalies in the extratropical North Pacific (Mantua et al., 1997), shifts its phase with periods from 20 to 30 years (Mantua and Hare, 2002). The potential to resolve meaningful winter monsoon variability within this frequency range with our record is, however, limited by the 9-year resolution and requires records capable of resolving inter-decadal signals. The multi-decadal cycles estimated by MTM are close to the 78- and 35-year periodicities found by Neff et al. (2001) for the Hoti cave (H5) $\delta^{18}\text{O}$ stalagmite record from northern Oman. Their record spans the early to mid-Holocene evolution of the Indian summer monsoon precipitation, and the decadal-scale variability is interpreted to be controlled by solar irradiance forcing. The 75-year periodicity is also very close to the ~79-year cycle found in the Oman upwelling record, implied by Gupta et al. (2005) to be coherent with a sunspot cycle. In the eastern Arabian Sea, Agnihotri et al. (2002) found a dominant 60- to 70-year periodicity in a record of Indian summer monsoon variability over the last millennium that appears to be solar forcing. From a study of coastal

climate proxies in Sri Lanka that are interpreted to be controlled by winter monsoon variability, ~64- and 28- to 32-year periodicities were found (Ranasinghe et al., 2013). These findings suggest that summer and winter monsoons modulated on the same decadal-scale frequency bands are most likely driven by changes of solar irradiance. Furthermore, early to mid-Holocene periodicities (Neff et al., 2001) also existed during the late Holocene.

Implications for late Holocene SST variability and monsoon evolution

Our 2000-year record of wSST in the northeastern Arabian Sea shows three stages of winter monsoon evolution. The first interval until 100 CE is marked by a relatively stable period of temperatures warmer than average (Figure 8), implying weak winter monsoon conditions. The subsequent stage, between 100 and 450 CE, is characterized by high winter monsoon variability where highly fluctuating wSST suggests a transition phase of winter monsoon strength until after 450 CE when a sudden cooling marks the onset of persistently enhanced winter monsoon conditions. During the relatively stable but colder third phase from 450 CE onward, the most obvious feature is a gradual warming toward 950 CE, where winter monsoon conditions are weakest within that interval, and a gradual strengthening thereafter.

In a previous paper (Böll et al., 2014), we also found three distinct phases of changing monsoon intensities during the last ~2400 years, although the timing compared with the present study is slightly different. The most obvious features of the alkenone record are an abrupt decrease in AM-SST around 250 CE and a persistent warming around 1050–1150 CE (Figure 10). In contrast to our newly developed record of foraminiferal-based wSST, the former shift occurred between the end of stable weak winter monsoon conditions at 100 CE and the onset of intensified winter conditions after 450 CE, during the transition phase. The warming phase around 1050–1150 CE occurs apparently ~100 years later in the alkenone record and also shows a longer duration as in the wSST record. This might indicate that the observed three distinct climate phases of colder and warmer temperatures had a different impact on the respective seasonal cycles and that changes during the inter-monsoon season did not occur simultaneously to variations of winter monsoon intensity. These phases could have been

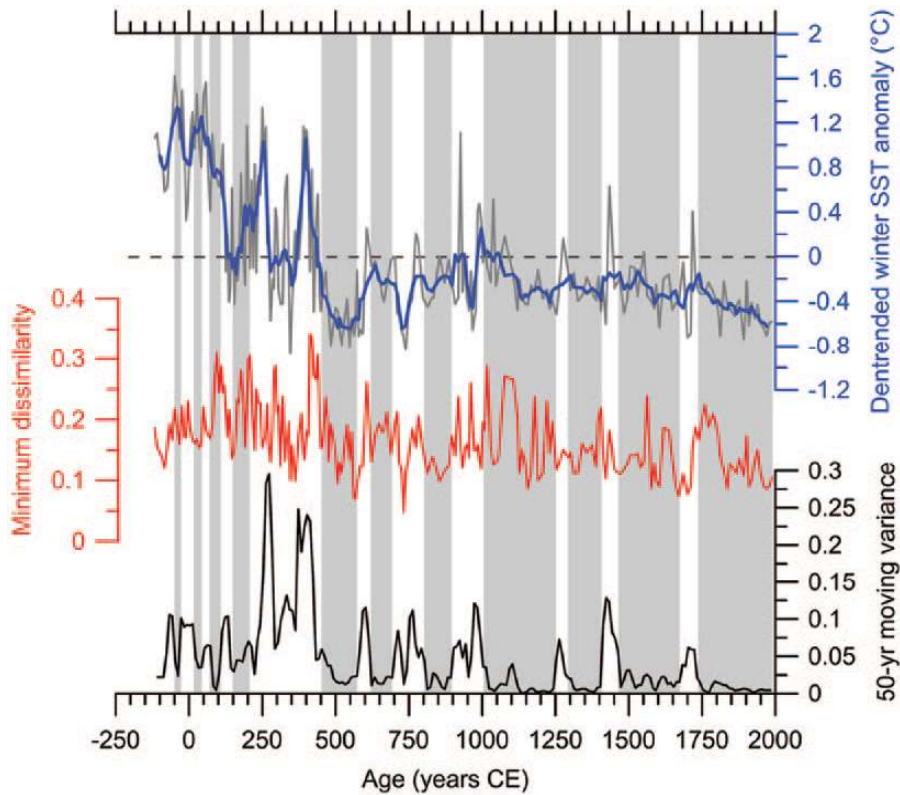


Figure 8. Temporal evolution of the wSST variance time series calculated within an overlapping 50-year moving window on the detrended time series filtered with a 30-year low-pass Butterworth filter. Gray bars indicate periods of low variance. Minimum Bray–Curtis dissimilarity between the fossil samples and the adjusted calibration dataset as a measure of analogy. Changes of winter monsoon intensity are shown as the detrended wSST anomaly.

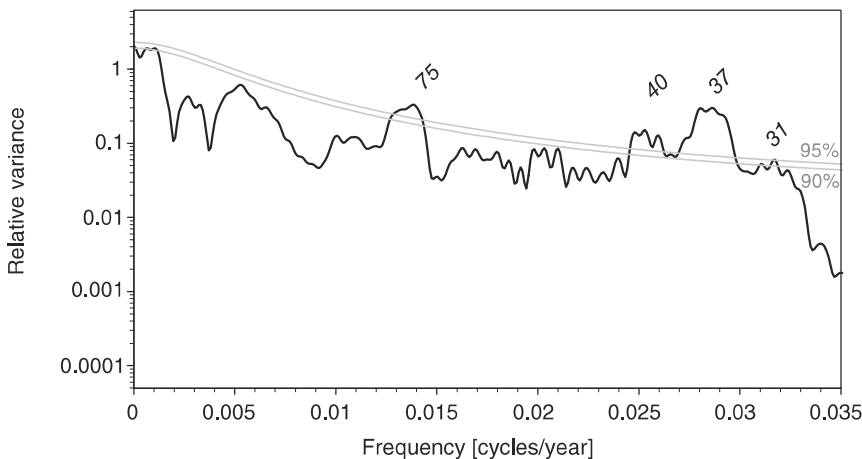


Figure 9. Results of a multitaper method (MTM) spectral analysis of the wSST record of winter monsoon variability over the last ~2000 years with a red noise null hypothesis (90% and 95% confidence levels are indicated as gray lines). Significant peaks are attributed to 75-, 40-, 37-, and 31-year cycles.

amplified in the AM-SST record because especially during intervals of weak winter monsoon intensity and accordingly warmer wSST, the contribution of the warmer inter-monsoon signal (cf. Figure 2, warmest modern SST > 27°C occur from April to November) to AM-SST must have been increased. Our data also do not indicate that winter conditions were substantially stronger at ~1800 CE, as it is evident from alkenone-derived AM-SST on the Pakistan Margin (Böll et al., 2014; Doose-Rolinski et al., 2001), a feature that was suggested to be linked to the ‘Little Ice Age’ (‘LIA’). Apparently, the colder ‘LIA’ climate only affected the inter-monsoon or summer temperatures in the northeastern Arabian Sea, without enhancing winter monsoon intensity. Furthermore, the observed difference of both climate series might,

apart from a potentially different control mechanism on the respective proxies, also be owed to the different sampling scheme of both records. Alkenone-derived AM-SST and foraminiferal-based wSST are co-registered in the same sediment core, but the record of AM-SST uses a continuous 25-year resolution, whereas the record of wSST is based on a continuous 9-year resolution. This especially explains the observed amplitudinal difference of both SST time series as the lower sampling resolution integrates almost three samples of the higher resolution record. However, resampling of both records to the lower sampling resolution following AM-SST by linear interpolation reveals a positive correlation ($r=0.60$, $p=4.44E-09$), indicating that winter temperatures must have a strong control on AM-SST.

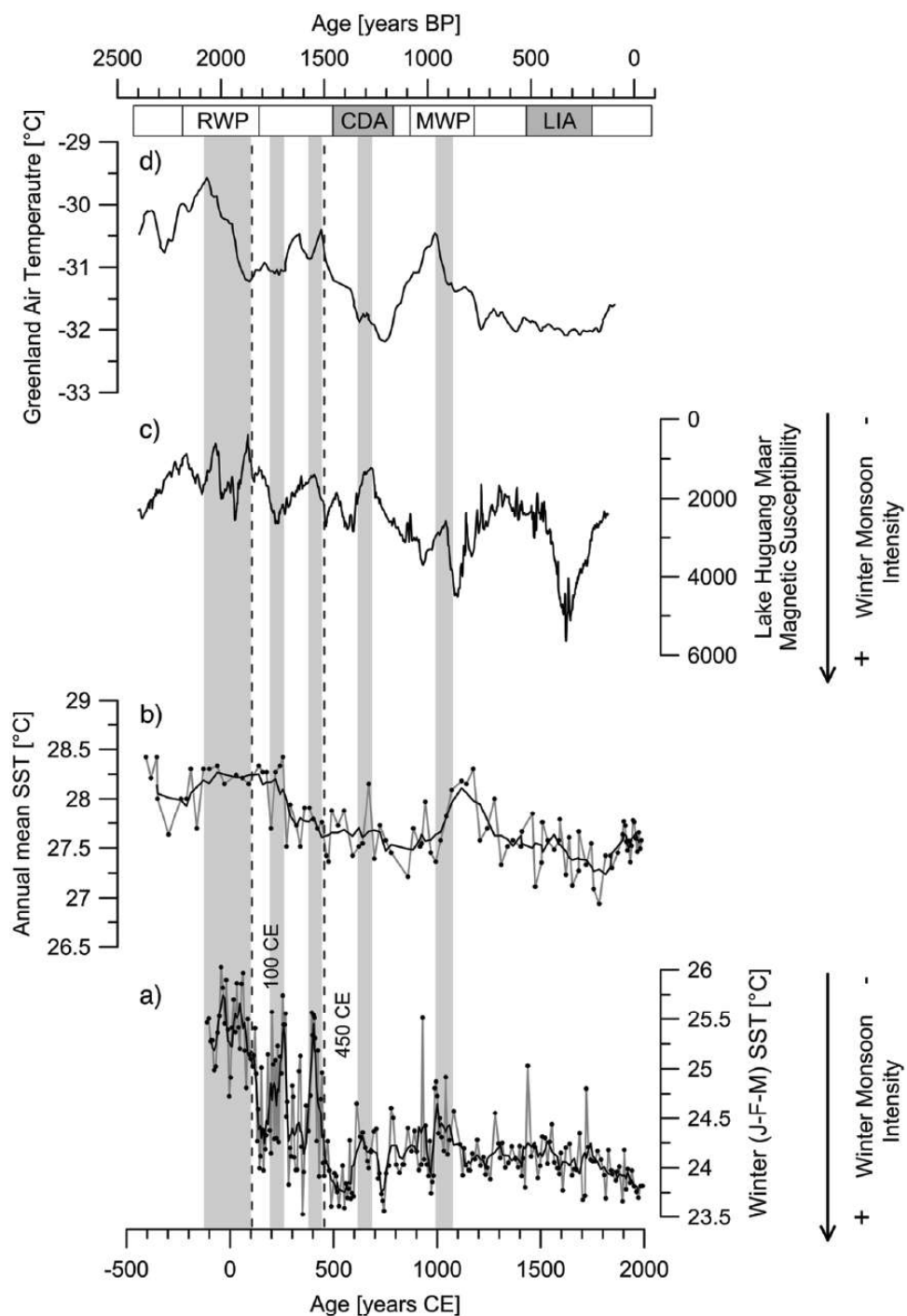


Figure 10. (a) Reconstructed winter sea surface temperatures (wSST) from cores 39KG/275KL during the last ~2000 years as the consensus from all transfer function methods (black line as 3-pt running mean) and (b) alkenone-derived annual mean temperatures co-registered in the same sediment core (Böll et al., 2014). (c) Magnetic susceptibility of Lake Huguang Maar (Yancheva et al., 2007) indicates East Asian winter monsoon intensity. (d) Northern Hemisphere climate epochs are derived from Greenland air temperatures (Alley, 2000). Conspicuous temperature changes occurred around 100 and 450 CE (dashed lines). Intervals of diminished winter monsoon intensity are gray shaded.

One yet unresolved question about the regional monsoon systems exists as to how the Indian and East Asian monsoon systems are related on decadal to centennial timescales during the late Holocene (e.g. Wang et al., 2005a, 2014). The Indian and East Asian monsoon systems react to different forcing mechanisms and are thus expected to reveal dissimilar variability of their proxy records (Wang et al., 2003). Because of the scarcity of high-resolution winter monsoon records, the relationship of both winter monsoon systems remains unclear. Although the temperature range of the wSST record of this study after 450 CE is mostly within the reconstruction uncertainty of ~1°C, persistent cold spells around 450–600 CE and 750 CE, as well as warmer

intervals between 600–700 CE, around 950 CE, 1300 CE, and 1450 CE, are consistent with the Lake Huguang Maar magnetic susceptibility record of East Asian winter monsoon intensity (Figure 10). This relationship is further investigated by wavelet coherence analysis (Figure 11) that measures the coherency of two cross wavelet transforms in time–frequency space (Grindsted et al., 2004), using the MATLAB package available on the website of the National Oceanography Centre (<http://noc.ac.uk/using-science/crosswavelet-wavelet-coherence>). A broad significant interval with the same phase angle shows a strong coherency between 100 BCE and 1000 CE at a period of 300–400 years. Further significant coherency on shorter wavelengths around 30–50 years occurs in

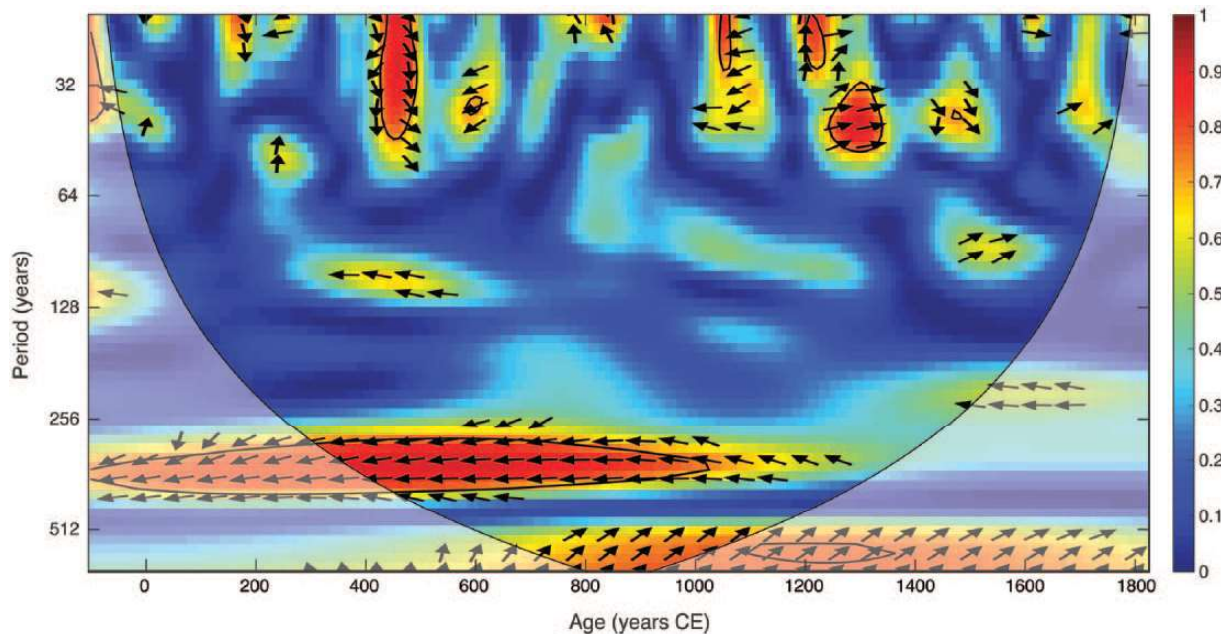


Figure 11. Wavelet coherency between the wSST record and magnetic susceptibility of the Lake Huguang Maar record (Yancheva et al., 2007) indicates areas in the time–frequency space where both time series covary. The colorbar units are wavelet squared coherencies, and the thick black contour shows the 5% significance level against red noise. The phase shift between the components of both time series is indicated within the significant areas by arrows (pointing right = in-phase, pointing left = anti-phase, up = wSST leading Lake Huguang Maar by 90°, down = Lake Huguang Maar leading wSST by 90°). Note that anti-phase behavior of both proxies means in-phase response to monsoon intensity, as increasing intensity is relative to opposite scaling. The cone of influence where edge artifacts might be introduced is indicated as white shading.

disconnected intervals and shows either in-phase (around 1300 CE) or phase-shifted (around 500 CE) relationships between the two records. Periodicities on these frequency bands are also evident from the MTM power spectrum of wSST variability (Figure 9). This implies that a persistent centennial-scale relationship between the variation of the Indian winter monsoon and the East Asian winter monsoon existed until 1000 CE.

Our data indicate that the Indian winter monsoon intensity shifted rapidly during the last two millennia. The shift from persistent weak to highly variable winter conditions at 100 CE is concomitant with the end of the Northern Hemisphere ‘Roman Warm Period’ (‘RWP’). This is followed by strongest winter conditions at ~500–600 CE, concomitant with the onset of the Cold Dark Ages (CDA) and Bond event 1 in the North Atlantic (Bond et al., 2001). Several studies of late Holocene monsoon activity indicate changing conditions around that time. A persistent link between warmer North Atlantic climate and weaker winter monsoon on centennial timescales during the late Holocene was also suggested by Böll et al. (2014). Lückge et al. (2001) proposed the ‘transition phase’ of highly fluctuating wSST after 100 CE to be an interval of summer monsoon domination while the winter monsoon was diminished. Stalagmite records from Qunf Cave in southern Oman show a prominent hiatus until ~550 CE, which potentially indicates very low summer monsoon precipitation (Fleitmann and Matter, 2009; Fleitmann et al., 2007). Very low summer monsoon-induced upwelling off the Oman coast at ~550 CE is also evidenced by Gupta et al. (2003) and Anderson et al. (2010). This finding may suggest that strongest winter monsoon conditions were contemporaneous with phases of weakened summer monsoon, indicating an anti-phase relationship between summer and winter monsoon intensity.

Slightly weakened winter monsoon intensities at 950 CE might be related to the ‘MWP’ of the Northern Hemisphere. A gradual weakening of the winter monsoon toward 950 CE is compatible to a broad increase in Oman upwelling intensity at 750–1350 CE (Gupta et al., 2003), whereas the picture is less clear for the cave records (e.g. Fleitmann and Matter, 2009; Wang et al., 2005b). If an anti-phase relationship persisted during the late

Holocene until present, we would also expect to see the same major change for the last 400 years as implied by Anderson et al. (2002). But during that period, wSST are very stable, indicating even a very recent strengthening of winter conditions from 1800 CE onward. Changing conditions during the last 400 years are, however, also not evident from the records of Böll et al. (2014) and Yancheva et al. (2007), suggesting that an inverse relationship between Indian summer and winter monsoons is not persistent to the present.

Conclusion

We analyzed PF species compositions from an optimized dataset, adjusted to the reconstruction of the decadal-scale variability of fossil assemblages from the northeastern Arabian Sea. RDA revealed that wSST has the strongest effect on the explanation of the modern PF species variation. Winter monsoon-induced hydrographic conditions are revealed by a strong negative relationship between temperature and chlorophyll-based productivity estimates. The uCbPM is a useful representation of the nutrient conditions during winter deep mixing.

Reconstruction outcomes for the last two millennia show a consistent pattern among the techniques, indicating that ecological changes of the fossil assemblages are primarily caused by the reconstructed variable. The most obvious feature from the record of reconstructed winter monsoon intensity is a sudden change from warm temperatures around 25°C prior to 450 CE toward temperatures below 24°C thereafter. This shift is contemporaneous with the end of the ‘RWP’ on the Northern Hemisphere and mainly associated with a shift in the faunal assemblage caused by the occurrence of *G. sacculifer* and *G. siphonifera*.

Our record can be divided into three main phases:

- Prior to 100 CE, warm and stable temperatures above 25°C were found, representing diminished winter monsoon conditions.
- From 100 to 450 CE, highly variable temperatures indicate a transition phase.

3. After 450 CE, winter temperatures are constantly lower. Highest temperatures during this interval occurred around 950 CE concomitant with the ‘MWP’.

These phases can be paralleled to changes in records of late Holocene summer monsoon intensity. Frequency analysis revealed that winter monsoon intensity was modulated on decadal-scale periodicities that are known from proxy records of Indian summer monsoon and interpreted to be solar irradiance forcing. An inverse relationship of winter and summer monsoon intensity during the last two millennia is indicated by simultaneous prominent phase shifts, but is not persistent during the last 400 years.

Acknowledgements

The following institutions and colleagues have provided untreated core top material for foraminiferal analyses: BGR Hannover (U von Stackelberg, U von Rad, A Lückge), IOW Warnemünde (R Endler), Univ. Kharagpur (AK Gupta), NIO Goa (A Paropkari), Univ. Cambridge (T Kiefer), Univ. Hamburg (Ch Betzler), Univ. Mainz (F Sirocko), Univ. Tübingen (Ch Hemleben, P Heinz), Univ. Utrecht (JW Zachariasse). Tatjana Epp, Dorothea Mosandl, and Patrick Schwarz are thankfully acknowledged for lab assistance. We thank two anonymous reviewers for their constructive comments that helped to improve the manuscript.

Funding

Funding was provided by the German Ministry of Education and Research (BMBF) grant 03G0806C (CARIMA). The data will be available at www.pangaea.de.

References

- Agnihotri R, Dutta K, Bhushan R et al. (2002) Evidence for solar forcing on the Indian monsoon during the last millennium. *Earth and Planetary Science Letters* 198 (3–4): 521–527.
- Aitchinson J (1999) Logratios and natural laws in compositional data analysis. *Mathematical Geology* 31(5): 563–580.
- Aitchinson J, Barcelo-Vidal C, Martin-Fernandez JA et al. (2000) Logratio analysis and compositional distance. *Mathematical Geology* 32(3): 271–275.
- Alley R (2000) Ice-core evidence of abrupt climate changes. *Proceedings of the National Academy of Sciences of the United States of America* 97: 1331–1334.
- Anderson DM, Overpeck JT and Gupta AK (2002) Increase in the Asian Southwest monsoon during the past four centuries. *Science* 297: 596–599.
- Anderson DM, Baulcomb CK, Duvivier AK et al. (2010) Indian summer monsoon during the last two millennia. *Journal of Quaternary Science* 25: 911–917.
- André A, Weiner A, Quillévéré F et al. (2013) The cryptic and the apparent reversed: Lack of genetic differentiation within the morphologically diverse plexus of the planktonic foraminifer *Globigerinoides sacculifer*. *Paleobiology* 39(1): 21–39.
- Auras-Schudnagies A, Kroon D, Ganssen G et al. (1989) Distributional pattern of planktonic foraminifers and pteropods in surface waters and top core sediments of the Red Sea, and adjacent areas controlled by the monsoonal regime and other ecological factors. *Deep-Sea Research* 36: 1515–1533.
- Banse K (1987) Seasonality of phytoplankton chlorophyll in the central and northern Arabian sea. *Deep-Sea Research Part A: Oceanographic Research Papers* 34: 713–723.
- Banse K and McClain CR (1986) Winter blooms of phytoplankton in the Arabian Sea as observed by the Coastal Zone Color Scanner. *Marine Ecology: Progress Series* 34: 201–211.
- Barrows TT and Juggins S (2005) Sea-surface temperatures around the Australian margin and Indian Ocean during the Last Glacial Maximum. *Quaternary Science Reviews* 24: 1017–1047.
- Bé AWH (1967) Foraminifera, families – Globigerinidae and Globorotaliidae, Fiche no. 108. In: Frasier JH (ed.) *Fiches d'intification du zooplankton*. Copenhagen: Conseil International pour l'Exploration de la Mer, pp. 1–8.
- Bé AWH (1977) An ecological, zoogeographic and taxonomic review of recent planktonic foraminifera. In: Ramsey ATS (ed.) *Oceanic Micropalaeontology*. London: Academic Press, Inc., pp. 1–100.
- Bé AWH and Hutson WH (1977) Ecology of planktonic foraminifera and biogeographic patterns of life and fossil assemblages in the Indian Ocean. *Micropaleontology* 23: 369–414.
- Behrenfeld MJ and Falkowski PG (1997) Photosynthetic rates derived from satellite-based chlorophyll concentration. *Limnology and Oceanography* 42: 1–20.
- Birks HJB, Line JM, Juggins S et al. (1990) Diatoms and pH reconstruction. *Philosophical Transactions of the Royal Society B: Biological Sciences* 327: 263–278.
- Böll A, Lückge A, Munz P et al. (2014) Late Holocene primary productivity and sea surface temperature variations in the northeastern Arabian Sea: Implications for winter monsoon variability. *Paleoceanography* 29: 778–794.
- Bond G, Kromer B, Beer J et al. (2001) Persistent solar influence on North Atlantic climate during the Holocene. *Science* 294: 2130–2136.
- Bräuning A and Mantwill B (2004) Summer temperature and summer monsoon history on the Tibetan plateau during the last 400 years recorded by tree rings. *Geophysical Research Letters* 31: L24205.
- Burns SJ, Fleitmann D, Mudelsee M et al. (2002) A 780-year annually resolved record of Indian Ocean monsoon precipitation from a speleothem from south Oman. *Journal of Geophysical Research: Atmospheres* 107(D20): 4434.
- Cayre O, Beaufort L and Vincent E (1999) Paleoproductivity in the equatorial Indian Ocean for the last 260,000 yr: A transfer function based on planktonic foraminifera. *Quaternary Science Reviews* 18: 839–857.
- Colborn JG (1975) *The Thermal Structure of the Indian Ocean: International Indian Ocean Expedition Oceanographic Monographs*, vol. 2. Honolulu, HI: University of Hawaii Press, p. 173.
- Conkright ME, Locarnini RA, Garcia HE et al (2002) *World Ocean Atlas 2001: Objective Analyses, Data Statistics, and Figures – CD-ROM Documentation*. National Oceanographic Data Center, Silver Spring, MD. Available at: http://odv.awi.de/fileadmin/user_upload/odv/data/WOA01/README.PDF.
- Cook E, Krusic P, Anchukaitis K et al. (2013) Tree-ring reconstructed summer temperature anomalies for temperate East Asia since 800 C.E. *Climate Dynamics* 41: 2957–2972.
- Currie RI, Fisher AE and Hargraves PM (1973) Arabian Sea upwelling. In: Zeitschel B and Gerlach SA (eds) *The Biology of the Indian Ocean*. Berlin: Springer-Verlag, pp. 37–52.
- Curry WB, Ostermann DR, Gupta MVS et al. (1992) Foraminiferal production and monsoonal upwelling in the Arabian Sea: Evidence from sediment traps. In: Summerhayes CP, Prell WL and Emeis KC (eds) *Upwelling Systems: Evolution since the Early Miocene*. London: Geological Society of London (Special Publications 64), pp. 93–106.
- Dixon P (2003) VEGAN, a package of R functions for community ecology. *Journal of Vegetation Science* 14: 927–930.
- Doose-Rolinski H, Rogalla U, Scheeder G et al. (2001) High-resolution temperature and evaporation changes during the late Holocene in the northeastern Arabian Sea. *Paleoceanography* 16: 358–367.
- Feldman GC and McClain CR (2013) *Ocean Color Web, SeaWiFS, AquaMODIS/Chlorophyll a Concentration* (ed N

- Kuring SW Bailey BA Franz). NASA Goddard Space Flight Center. Available at: <http://oceancolor.gsfc.nasa.gov/>.
- Fleitmann D and Matter A (2009) The speleothem record of climate variability in Southern Arabia. *Comptes Rendus Geoscience* 341: 633–642.
- Fleitmann D, Burns SJ, Mangini A et al. (2007) Holocene ITCZ and Indian monsoon dynamics recorded in stalagmites from Oman and Yemen (Socotra). *Quaternary Science Reviews* 26: 170–188.
- Fleitmann D, Burns SJ, Mudelsee M et al. (2003) Holocene forcing of the Indian monsoon recorded in a stalagmite from southern Oman. *Science* 300: 1737–1739.
- Fraile I, Schulz M, Multizzi S et al. (2008) Predicting the global distribution of planktonic foraminifera using a dynamic ecosystem model. *Biogeosciences* 5: 891–911.
- Ghil M, Allen RM, Dettinger MD et al. (2002) Advanced spectral methods for climatic time series. *Reviews of Geophysics* 40: 1–41.
- Grindsted A, Moore JC and Jevrejeva S (2004) Application of the cross wavelet transform and wavelet coherence to geophysical time series. *Nonlinear Processes in Geophysics* 11: 561–566.
- Gupta AK, Anderson DM and Overpeck JT (2003) Abrupt changes in the Asian southwest monsoon during the Holocene and their links to the North Atlantic Ocean. *Nature* 421: 354–357.
- Gupta AK, Das M and Anderson DM (2005) Solar influence on the Indian summer monsoon during the Holocene. *Geophysical Research Letters* 32: L17703.
- Hemleben C, Spindler M and Anderson RO (1989) *Modern Planktonic Foraminifera*. New York: Springer-Verlag, 363 pp.
- Horn JL (1965) A rationale and test for the number of factors in factor analysis. *Psychometrika* 30: 179–185.
- Hutson WH and Prell WL (1980) A paleoecological transfer function, FI-2, for Indian Ocean planktonic foraminifera. *Journal of Paleontology* 54: 381–399.
- Imbrie J and Kipp NG (1971) A new micropaleontological method for quantitative paleoclimatology: Application to a late Pleistocene Caribbean core. In: Turekian KK (ed.) *Late Cenozoic Glacial Ages*. New Haven, CT: Yale University Press, pp. 71–181.
- Ittekkot V, Haake B, Bartsch M et al. (1992) Organic carbon removal in the sea: The continental connection. In: Summerhayes CP, Prell WL and Emeis KC (eds) *Upwelling Systems: Evolution since the Early Miocene*. London: Geological Society of London (Special Publications 64), pp. 167–176.
- Jolliffe IT (2002) *Principal Component Analysis*. New York: Springer, 488 pp.
- Jones PD and Mann ME (2004) Climate over the past millennia. *Reviews of Geophysics* 42(2): RG2002.
- Juggins S (2013) rioja: Analysis of Quaternary science data (R package version (0.8-7)). Available at: <http://cran.r-project.org/package=rioja>.
- Juggins S and Birks HJB (2012) Quantitative environmental reconstructions from biological data. In: Birks HJB, Lotter AF, Juggins S et al. (eds) *Tracking Environmental Change Using Lake Sediments*. New York: Springer, pp. 431–494.
- Kemp AES (1996) *Paleoclimatology and Paleoceanography from Laminated Sediments*. London: Geological Society of London (Special Publications 116), 258 pp.
- Kim J-W, Yeh S-W and Chang E-C (2014) Combined effect of El Niño-Southern Oscillation and Pacific Decadal Oscillation on the East Asian winter monsoon. *Climate Dynamics* 42: 957–971.
- Krishnamurthy L and Krishnamurthy V (2014) Influence of PDO on South Asian summer monsoon and monsoon–ENSO relation. *Climate Dynamics* 42: 2397–2410.
- Kucera M, Rosell-Melé A, Schneider R et al. (2005a) Multiproxy approach for the reconstruction of the glacial ocean surface (MARGO). *Quaternary Science Reviews* 24(7–9): 813–819.
- Kucera M, Weinelt M, Kiefer T et al. (2005b) Reconstruction of sea-surface temperatures from assemblages of planktonic foraminifera: Multi-technique approach based on geographically constrained calibration data sets and its application to glacial Atlantic and Pacific Oceans. *Quaternary Science Reviews* 24(7–9): 951–998.
- Kumar KK, Rajagopalan B, Hoerling M et al. (2006) Unraveling the mystery of Indian monsoon failure during El Niño. *Science* 314: 115–119.
- Lal D (ed.) (1994) Biogeochemistry of the Arabian Sea. *Proceedings, Indian Academy of Sciences (Earth and Planetary Sciences)* 103(2): 99–106.
- Laskar AH, Yadava MG, Ramesh R et al. (2013) A 4 kyr stalagmite oxygen isotopic record of the past Indian Summer Monsoon in the Andaman Islands. *Geochemistry, Geophysics, Geosystems* 14: 3555–3566.
- Lückge A, Doose-Rolinski H, Khan AA et al. (2001) Monsoonal variability in the northeastern Arabian Sea during the past 5000 years: Geochemical evidence from laminated sediments. *Palaeogeography, Palaeoclimatology, Palaeoecology* 167: 273–286.
- Lückge A, Reinhardt L, Andrleit H et al. (2002) Formation of varve-like laminae off Pakistan: Decoding 5 years of sedimentation. *Special Publication: Geological Society of London* 195: 421–431.
- Madhupratap M, Prasanna Kumar S, Bhattachari PMA et al. (1996) Mechanism of the biological response to winter cooling in the northeastern Arabian Sea. *Nature* 384: 549–552.
- Malmgren BA and Nordlund U (1997) Application of artificial neural networks to paleoceanographic data. *Palaeogeography, Palaeoclimatology, Palaeoecology* 136: 359–373.
- Mantua NJ and Hare SJ (2002) The Pacific decadal oscillation. *Journal of Oceanography* 58: 35–44.
- Mantua NJ, Hare SR, Zhang Y et al. (1997) A Pacific interdecadal climate oscillation with impacts on salmon production. *Bulletin of the American Meteorological Society* 78: 1069–1079.
- Morey AE, Mix AC and Pisias NG (2005) Planktonic foraminiferal assemblages preserved in surface sediments correspond to multiple environmental variables. *Quaternary Science Reviews* 24: 925–950.
- Murty VSN, Sarma YVB, Rao DP et al. (1992) Water characteristics, mixing and circulation in the Bay of Bengal during southwest monsoon. *Journal of Marine Research* 50: 207–228.
- Naidu PD and Malmgren BA (1996) A high-resolution record of late Quaternary upwelling along the Oman Margin, Arabian Sea based on planktonic foraminifera. *Paleoceanography* 11: 129–140.
- Neff U, Burns SJ, Mangini A et al. (2001) Strong coherence between solar variability and the monsoon in Oman between 9 and 6 kyr ago. *Nature* 411: 290–293.
- Ocean Productivity Site (2014) Oregon State University. Available at: <http://www.science.oregonstate.edu/ocean/productivity/index.php>.
- PAGES 2k Consortium (2013) Continental-scale temperature variability during the past two millennia. *Nature Geoscience* 6: 339–346.
- Peeters FJC and Brummer GJA (2002) The seasonal and vertical distribution of living planktic foraminifera in the NW Arabian Sea. In: Clift PD, Kroon D, Gaedicke C et al (eds) *The Tectonic and Climatic Evolution of the Arabian Sea Region*. London: Geological Society of London (Special Publications 195), pp. 463–498.
- Prasanna Kumar S, Ramaiah N, Gauns M et al. (2001) Physical forcing of biological productivity in the Northern Arabian Sea

- during the Northeast Monsoon. *Deep-Sea Research Part II: Topical Studies in Oceanography* 48: 1115–1126.
- R Core Team (2014) *R: A Language and Environment for Statistical Computing*. Vienna: R Foundation for Statistical Computing. Available at: <http://www.R-project.org>.
- Ramette A (2007) Multivariate analyses in microbial ecology. *FEMS Microbiology Ecology* 62(2): 142–160.
- Ranasinghe PN, Ortiz JD, Smith AJ et al. (2013) Mid- to late-Holocene Indian winter monsoon variability from a terrestrial record in eastern and southeastern coastal environments of Sri Lanka. *The Holocene* 23(7): 945–960.
- Schiebel R, Zeltner A, Treppke UF et al. (2004) Distribution of diatoms, coccolithophores and planktic foraminifers along a trophic gradient during SW monsoon in the Arabian Sea. *Marine Micropaleontology* 51: 345–371.
- Schlitzer R (2014) Ocean Data View. Available at: <http://odv.awi.de>.
- Schulz H and von Rad U (2014) Vertical and lateral flux on the continental slope off Pakistan: Correlation of sediment core and trap results. *Biogeosciences* 11: 3107–3120.
- Schulz H, von Rad U and Ittekkot V (2002) Planktic foraminifera, particle flux and oceanic productivity off Pakistan, NE Arabian Sea: Modern analogues and application to the paleoclimatic record. In: Clift PD, Kroon D, Gaedicke C et al. (eds) *The Tectonic and Climatic Evolution of the Arabian Sea Region*. London: Geological Society of London (Special Publications 195), pp. 499–516.
- Schulz H, von Rad U and von Stackelberg U (1996) Laminated sediments from the oxygen-minimum zone of the northeastern Arabian Sea. In: Kemp AES (ed.) *Paleoclimatology and Paleoceanography from Laminated Sediments*. London: Geological Society of London (Special Publications 116), pp. 185–207.
- Shetye SR, Gouveia AD and Shenoi SSC (1994) Circulation and water masses of the Arabian Sea. In: Lal D (ed.) *Biogeochemistry of the Arabian Sea: Proceedings, Indian Academy of Sciences (Earth and Planetary Sciences)* 103(2): 9–25.
- Siccha M, Trommer G, Schulz H et al. (2009) Factors controlling the distribution of planktonic foraminifera in the Red Sea and implications for the development of transfer functions. *Marine Micropaleontology* 72: 146–156.
- Smith S, Roman M, Prusova I et al. (1998) Seasonal response of zooplankton to monsoonal reversals in the Arabian Sea. *Deep-Sea Research Part II: Topical Studies in Oceanography* 45: 2369–2403.
- Sontakke NA, Pant GB and Singh N (1993) Construction of all-India summer monsoon rainfall series for the period 1844–1991. *Journal of Climate* 6: 1807–1811.
- Telford RJ and Birks HJB (2005) The secret assumption of transfer functions: Problems with spatial autocorrelation in evaluating model performance. *Quaternary Science Reviews* 24: 2173–2179.
- Telford RJ, Li C and Kucera M (2013) Mismatch between the depth habitat of planktonic foraminifera and the calibration depth of SST transfer functions my bias reconstructions. *Climate of the Past* 9: 859–870.
- Telford RJ, Andersson C, Birks HJB et al. (2004) Biases in the estimation of transfer function prediction errors. *Paleoceanography* 19: PA4014.
- ter Braak CJF and Juggins S (1993) Weighted averaging partial least squares regression (WA-PLS): An improved method for reconstructing environmental variables from species assemblages. *Hydrobiologia* 269–270: 485–502.
- von Rad U, Doose H and Cruise Participants (1998) *SONNE Cruise SO 130 Cruise Report MAKRAN II*. Hannover: Bundesanstalt für Geowissenschaften und Rohstoffe.
- von Rad U, Schulz H and SONNE 90 Scientific Party (1995) Sampling the oxygen minimum zone off Pakistan: Glacial-interglacial variations of anoxia and productivity (preliminary results, SONNE 90 cruise). *Marine Geology* 125: 7–19.
- von Rad U, Schaaf M, Michels KH et al. (1999) A 5000-yr record of climate change in varved sediments from the oxygen minimum zone off Pakistan, Northeastern Arabian Sea. *Quaternary Research* 51: 39–53.
- Wang B, Clemens SC and Liu P (2003) Contrasting the Indian and East Asian monsoons: Implications on geologic timescales. *Marine Geology* 201: 5–21.
- Wang P, Clemens S, Beaufort L et al. (2005a) Evolution and variability of the Asian monsoon system: State of the art and outstanding issues. *Quaternary Science Reviews* 24(5–6): 595–629.
- Wang PX, Wang B, Cheng H et al. (2014) The global monsoon across timescales: Coherent variability of regional monsoons. *Climate of the Past* 10: 2007–2052.
- Wang Y, Cheng H, Edwards RL et al. (2005b) The Holocene Asian monsoon: Links to solar changes and North Atlantic climate. *Science* 308: 854–857.
- Webster PJ, Magaña VO, Palmer TN et al. (1998) Monsoons: Processes, predictability, and the prospects for prediction. *Journal of Geophysical Research: Oceans* 103(C7): 14451–14510.
- Weiner AKM, Weinkauf MFG, Kurasawa A et al. (2015) Genetic and morphometric evidence for parallel evolution of the *Globigerinella calida* morphotypes. *Marine Micropaleontology* 114: 19–35.
- Wyrtki K (1971) *Oceanographic Atlas of the International Indian Ocean Expedition*. Washington, DC: National Science Foundation.
- Wyrtki K (1973) Physical oceanography of the Indian Ocean. In: eitschel B and Gerlach SA (eds) *The Biology of the Indian Ocean*. New York: Springer, pp. 18–36.
- Xu H, Hong Y and Hong B (2012) Decreasing Asian summer monsoon intensity after 1860 AD in the global warming epoch. *Climate Dynamics* 39: 2079–2088.
- Yancheva G, Nowaczyk NR, Mingram J et al. (2007) Influence of the intertropical convergence zone on the East Asian monsoon. *Nature* 445: 74–77.
- Zeitschel B and Gerlach SA (1973) *The Biology of the Indian Ocean*. Berlin: Springer-Verlag, 549 pp.
- Zhou W, Wang X, Zhou TJ et al. (2007) Interdecadal variability of the relationship between the East Asian winter monsoon and ENSO. *Meteorology and Atmospheric Physics* 98(3–4): 283–293.